Association of the AB and CD-EF Domains from Rat α- and β-Parvalbumin†

Michael T. Henzl,* Sayeh Agah, and John D. Larson

Department of Biochemistry, University of Missouri—Columbia, Columbia, Missouri 65211

Received April 14, 2004; Revised Manuscript Received June 21, 2004

ABSTRACT: Association of the parvalbumin AB and CD-EF domains was examined in Hepes-buffered saline, pH 7.4, employing fragments from rat α and β. All of the interactions require Ca^{2+}. In saturating Ca^{2+}, the α AB/α CD-EF (α/α) complex displays an association constant of $(7.6 \pm 0.4) \times 10^7$ M^{-1}. Ca^{2+}-binding data for a mixture of the α fragments are compatible with an identical two-site model, yielding an average binding constant of $(8.5 \pm 0.2) \times 10^5$ M^{-1}. The β/β interaction is significantly weaker, exhibiting an association constant of $(3.0 \pm 0.6) \times 10^6$ M^{-1}. The Ca^{2+}-binding constants for β/β are likewise diminished, at $(1.0 \pm 0.1) \times 10^5$ and $(2.3 \pm 0.2) \times 10^4$ M^{-1}. The magnitude of the apparent $\Delta\Delta G°'$ for Ca^{2+} binding by α/α and β/β, at 3.4 kcal/mol, approaches that measured for the intact proteins (3.6 kcal/mol) and is substantially larger than the 1.5 kcal/mol value previously measured for the isolated CD-EF domains. This result suggests that the AB domain can modulate the Ca^{2+} affinities of the CD and EF sites. Interestingly, the heterologous α/β complex displays a larger association constant [$(6.6 \pm 0.4) \times 10^6$ M^{-1}] than the homologous β/β complex and heightened Ca^{2+} affinity [binding constants of $(1.3 \pm 0.1) \times 10^6$ and $(8.8 \pm 0.2) \times 10^4$ M^{-1}]. By contrast, β/α associates more weakly than α/α and exhibits sharply reduced affinity for Ca^{2+}. Thus, the interaction between the β AB domain and β CD-EF domain may act to attenuate Ca^{2+} affinity in the intact protein.

EF-hand proteins are essential participants in Ca^{2+}-dependent signal transduction pathways (*1*−*3*). The EF-hand metal ion-binding motif consists of a 12-residue central binding loop flanked by short α helices (*1*, *4*−*6*). The ligands are arrayed in pseudooctahedral fashion around the metal ion and are referenced by the axes of a Cartesian coordinate system. The side chains of loop residues 1, 3, and 5 furnish the $+x$, $+y$, and $+z$ ligands. The main-chain carbonyl of loop residue 7 serves as the $-y$ ligand, and water is frequently the proximal ligand at $-x$. A nearly invariant glutamyl side chain occupies the $-z$ position. When Ca^{2+} occupies the binding site, the $-z$ coordination is bidentate, so that the coordination is actually pentagonal bipyramidal. By contrast, Mg^{2+} is coordinated in a monodentate fashion at $-z$ (*7*).

After nearly 3 decades of inquiry, the energetics of EF-hand metal ion-binding affinity remain incompletely understood. The mammalian α- and β-parvalbumin (PV)[1] isoforms offer an attractive system for addressing this issue. Parvalbumins are small (M_r 12000), vertebrate-specific proteins that function as cytosolic Ca^{2+} buffers (*8*, *9*). They contain two metal ion-binding sites, the CD and EF sites (Figure 1A). The X-ray crystallographic structure of carp PV established the EF-hand paradigm (*11*), and the motif is named after the EF site in that protein.

Despite 49% sequence identity (*12*, *13*), the two PV isoforms from rat exhibit very distinct divalent ion-binding properties. Whereas both binding sites in rat α-PV are high-affinity sites, the rat β-PV CD site is a low-affinity site (*14*−*17*). Evidence has accumulated to suggest that the disparate metal ion-binding behavior is dictated by structural differences both within and outside the ion-binding loops.

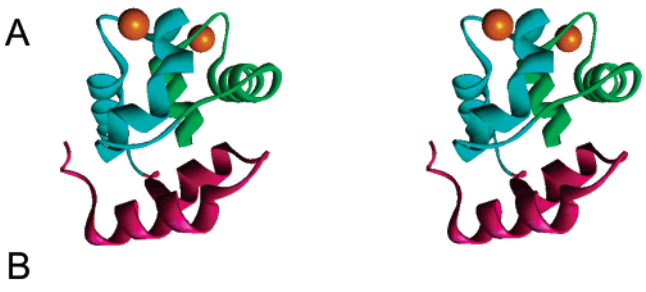

FIGURE 1: (A) The parvalbumin fold. Stereoscopic view of the peptide backbone of Ca^{2+}-bound rat β-parvalbumin. The AB domain (residues 1−37) is colored magenta, residues 38−75 (including the CD binding site) are in cyan, residues 76−108 (including the EF site) are in green, and the two bound Ca^{2+} ions are in orange. Coordinates are from Ahmed et al. (*10*). This figure was prepared with WebLab ViewerLite 3.20 (Molecular Simulations Inc.). (B) Sequence comparison of the rat α and β AB domains. Data are from refs *12* and *13*, respectively.

A previous study from this laboratory compared the physical and divalent ion-binding properties of the CD-EF metal ion-binding domains of rat α and β (*18*). This paper examines the association of the AB and CD-EF fragments of the two proteins at saturating levels of Ca^{2+} and compares the apparent Ca^{2+} affinities of the resulting AB/CD-EF complexes. Data for the heterologous AB/CD-EF complexes are also presented. Permyakov et al. previously used this

† This work was supported by NSF Award MCB0131166 (to M.T.H.).

* Corresponding author. Tel: 573-882-7485. Fax: 573-884-4812. E-mail: henzlm@missouri.edu.

10.1021/bi049254d CCC: $27.50
Published on Web 08/04/2004

approach to study the association of the AB and CD-EF fragments from pike α-parvalbumin (*19*).

MATERIALS AND METHODS

AB Fragments. The AB fragments were produced as fusion proteins, employing rat *β*-PV as the fusion partner. Rat *β* was chosen for its high expression level and for its diminutive size, which would facilitate proteolytic removal of the AB peptide and produce a higher molar yield of recombinant protein. The rat *β* sequence, cloned between the *Nde*I and *Bam*HI sites in pET11 (Novagen), was modified to serve as a fusion host by removing the stop codon and inserting an *Nco*I site using the QuikChange mutagenesis kit (Stratagene). The resulting construction was called pET11-BNCO. All PCR amplifications described herein employed *Pfu* Turbo polymerase (Stratagene), a high-fidelity thermostable DNA polymerase.

Coding information for the rat α and *β* AB fragments (residues 1−37) was amplified from the full-length cDNA sequences. The antisense PCR primers employed for amplification also introduced a stop codon after residue 37 and a 3′ *Bam*HI site. The resulting amplification products were cloned into pCR2.1 using the TOPO-TA cloning kit (Invitrogen). A consensus thrombin recognition site (ThRS, Leu-Val-Pro-Arg-Gly) and decahistidine tag (His_{10}) were then introduced immediately upstream from the codon for residue 1 (serine in both α and *β*) via four rounds of PCR amplification. The final sense PCR primer also introduced an *Nco*I site at the 5′ end of the construct. The resulting *Nco*I-His_{10}-ThRS-PV_{1-37} fragments were captured in pCR2.1. Following release with *Nco*I and *Bam*HI, they were ligated into pET11-BNCO that had been similarly digested. The resulting expression vectors were named pET11BNCO-αAB and pET11BNCO-*β*AB. The fidelity of all PV coding information in these constructs was verified by automated DNA sequencing.

For expression, the pET11BNCO-αAB and -*β*AB vectors were transformed into *Escherichia coli* BL21(DE3). One liter cultures (LB broth, 100 *μ*g/mL ampicillin) were induced with 0.25 mM IPTG when the absorbance at 600 nm reached 0.5. After an additional 2 h at 37 °C, the cell paste was collected by centrifugation. Cells were lysed with BugBuster reagent (Novagen), 5 mL/gram of cell paste.

Following clarification, the lysate was loaded, at 4 °C, onto Ni-NTA−agarose (Novagen, 5 mL column bed), equilibrated with NaCl−NaP_i buffer (0.30 M NaCl and 0.05 M NaP_i, pH 8.0), containing 0.01 M imidazole. After weakly bound proteins were washed off with NaCl−NaP_i buffer containing 0.02 M imidazole, the fusion protein was eluted with 0.25 M imidazole in NaCl−NaP_i buffer. The eluate was concentrated to 2 mL by ultrafiltration and then subjected to gel filtration on Sephadex G25 (40 mL column bed) at 4 °C in 0.15 M NaCl and 0.025 M Hepes, pH 7.4, containing 0.002 M Ca^{2+}.

Protein-containing fractions were pooled and treated overnight with thrombin (Novagen, 1 unit/mg of protein) at room temperature. Unavoidably, the AB fragments produced by thrombin cleavage contained an artifactual glycyl residue at the N-terminus. However, because tissue-derived parvalbumins are N-acetylated, the presence of the glycine was considered a relatively minor structural perturbation. SDS−PAGE analysis was used to confirm that the thrombin cleavage was complete.

After the NaCl concentration was increased to 0.30 M by addition of 2 M NaCl, the cleavage reaction was passed once again over Ni-NTA−agarose. The rat *β*-PV fusion partner, still harboring the decahistidine tag, was retained; the liberated AB fragment remained in the eluate. Following dialysis against 0.02 M Hepes−NaOH, pH 7.4, the eluate was loaded onto a 4 mL column of DEAE-Sepharose and then eluted with 0.5 M NaCl.

This strategy yielded *β* AB that was homogeneous by SDS−PAGE and mass spectrometry. Unfortunately, the α AB product was invariably truncated between residues 21−25, presumably due to proteolysis in culture, necessitating the use of a commercially synthesized peptide preparation (Global Peptide Services, Fort Collins, CO). The purity of the latter exceeded 95%, as judged by reverse-phase HPLC and mass spectrometry. Synthetic *β* AB was also obtained from the same company to compare the behavior of synthetic and recombinant preparations.

When analyzed by MALDI-TOF mass spectrometry, the synthetic α AB fragment displays a mass of 4094 Da, close to the predicted value of 4091 Da. The mass of the synthetic *β* fragment, 4055 Da, likewise displays good agreement with the predicted value of 4045 Da. By contrast, the mass of the recombinant preparation is 4101 Da, consistent with the anticipated presence of glycine at the N-terminus. The CD spectra for the α- and *β*-AB fragments are similar, both exhibiting a shoulder near 220 nm, suggestive of residual helical content, and a minimum near 200 nm.

CD-EF Fragments. The cloning and expression of the rat α and *β* CD-EF fragments, including residues 38−109 and 38−108, respectively, have been described elsewhere (*18*).

Analytical Ultracentrifugation. Sedimentation equilibrium was performed at 20 °C in a Beckman Optima XL-I analytical ultracentrifuge using an An50-Ti rotor. Samples were dialyzed against reference buffer (0.15 M NaCl and 0.025 M Hepes, pH 7.4) prior to analysis and loaded into six-channel charcoal-filled epon centerpieces. For samples containing the *β* AB fragment, the dialysis buffer contained 0.001 M tris(2-carboxyethyl)phosphine (TCEP, Pierce Biotechnology). The reference buffer also contained 0.001 M Ca^{2+} or 0.001 M EDTA, as required. Radial solute distributions, monitored at 257 nm, were collected at 1 h intervals until successive data sets were superimposable. In select

[1] Abbreviations: AB, the N-terminal parvalbumin domain, which includes the A and B helices; AB/CD-EF, the intermolecular complex formed by the parvalbumin AB and CD-EF fragments; CD, circular dichroism; CD site, the parvalbumin metal ion-binding site containing the C and D helices; CD-EF, the parvalbumin metal ion-binding domain, which includes the CD and EF sites; DTT, dithiothreitol; EDTA, ethylenediaminetetraacetic acid; EF site, the parvalbumin metal ion-binding site containing the E and F helices; Hepes, 4-(2-hydroxyethyl)-1-piperazineethanesulfonic acid; His_{10}, decahistidine affinity tag; LB, Luria−Bertani; HPLC, high-performance liquid chromatography; MALDI-TOF, matrix-assisted laser desorption ionization time of flight; Ni-NTA, nickel nitrilotriacetic acid; NMR, nuclear magnetic resonance; P_i, phosphate; PV, parvalbumin; SDS−PAGE, sodium dodecyl sulfate−polyacrylamide gel electrophoresis; TCEP, tris(carboxyethyl)phosphine; ThRS, thrombin recognition site; α/α, shorthand notation for the AB/CD-EF complex formed by the rat α fragments; *β*/*β*, shorthand for the corresponding rat *β* complex; α/*β*, shorthand for the complex formed from the α AB and *β* CD-EF fragments; *β*/α, shorthand for the complex formed by *β* AB and α CD-EF.

cases, the solute distribution was also monitored with interference optics.

Global least-squares analyses were performed with ORIGIN (OriginLab), version 5.0, employing the following equation, which describes the radial distribution of a single ideal species (*20*):

$$c = c_o \exp\left[\frac{M\omega^2(1-\bar{\nu}\rho)}{2RT}(r^2 - r_o^2)\right] + \mathrm{BL} \qquad (1)$$

In this relationship, c is the macromolecular solute concentration; r is the radial position; c_o is the solute concentration at an arbitrary radial position, r_o; M is the molecular weight of the solute; ω is the angular velocity; $\bar{\nu}$ is the partial specific volume of the solute, assumed to be 0.73 cm^3/g; ρ is the solvent density, 1.001 g/cm^3; R is the gas constant; T is the absolute temperature; and BL is a baseline offset to correct for minor optical mismatch between sample and reference cells. The angular velocity equals 2πRPM/60, where RPM is the rotor speed in revolutions per minute. M, c_o, and BL were varied to obtain the best agreement between observed and calculated values. M was a shared (or global) parameter; c_o and BL were unshared (or local) parameters.

Isothermal Titration Calorimetry. All titrations were conducted with a VP-ITC calorimeter (MicroCal) at 25 °C in 0.15 M NaCl and 0.025 M Hepes, pH 7.4. For experiments involving the β AB domain, DTT (0.001 M) was included in the buffer. A preinjection (2 μL) was included in each titration protocol. The heat associated with that titrant addition, artifactually low due to titrant diffusion during the thermal equilibration period, was ignored in the subsequent least-squares analysis. For titrations that reached an end point, the injection heats associated with the final additions were averaged to obtain an estimate of the heat of mixing. Otherwise, the heat of mixing and titrant dilution were estimated from a blank titration, i.e., injections of ligand into buffer. In either case, data were corrected for the mixing heat prior to fitting.

Divalent metal ions were removed from proteins, peptides, and buffers by passage over EDTA-derivatized agarose, at 4 °C, as described elsewhere (*18*). The residual Ca^{2+} content in the CD-EF preparations, measured by flame atomic absorption spectrometry, was less than 0.02 equiv.

Except for the titration of the β AB/β CD-EF mixtures with Ca^{2+}, all of the ITC data described below were modeled with fitting routines supplied by MicroCal. Association of the AB and CD-EF fragments, in the presence of saturating Ca^{2+}, was analyzed with a single-site model. Ca^{2+} binding by the AB/CD-EF complex was analyzed either with an independent two-site model or, if there was evidence of positive macroscopic cooperativity, with a two-site Adair model.

A somewhat more complex model was required to describe Ca^{2+} binding by an equimolar mixture of the β AB and β CD-EF fragments. In addition to Ca^{2+}-free CD-EF (M), CaAB/CD-EF (singly bound complex, XMY), and Ca_2AB/CD-EF (fully bound complex, X_2MY), the presence of CaCD-EF (XM) was also explicitly included. At the concentrations employed in these studies, the dimeric form of the unliganded CD-EF fragment (M_2) is negligibly populated, and inclusion of the dimeric singly bound species, $(XM)_2$, did not improve the fit. Thus, the minimal partition function required to satisfactorily fit this system is expressed by the equations:

$$\mathrm{PF} = \mathrm{M} + \mathrm{XM} + \mathrm{XMY} + \mathrm{X_2MY} \qquad (2)$$

$$\mathrm{PF} = \mathrm{M} + K_{10}\mathrm{M}x + K_{11}K_{10}\mathrm{M}xy + K_{21}K_{11}K_{10}\mathrm{M}x^2y \qquad (3)$$

In eq 3, x is the free Ca^{2+} concentration, y is the concentration of free β AB, K_{10} describes the binding of Ca^{2+} to CD-EF, K_{11} describes binding of the β AB fragment by CaCD-EF, and K_{21} describes the binding of the second Ca^{2+} by the CaAB/CD-EF complex.

Following the ith addition of Ca^{2+}, the expression for the cumulative heat of binding equals

$$Q_i = M_t V_o[H_{10}K_{10}x + (H_{11} + H_{10})(K_{11}K_{10}xy) + (H_{21} + H_{11} + H_{10})(K_{21}K_{11}K_{10}x^2y)]/\mathrm{PF} \qquad (4)$$

where M_t is the total CD-EF concentration, V_o is the calorimeter sample cell volume, H_{10} is the enthalpy change for the first Ca^{2+}-binding event, H_{11} is the enthalpy change associated with binding of the AB fragment to CaCD-EF, and H_{21} is the enthalpy change for binding of the second Ca^{2+} to the CaAB/CD-EF complex.

The heat associated with the ith injection equals the difference in the cumulative heats for the ith and $(i-1)$th injections, plus a correction for the volume displaced from the sample chamber by addition of titrant (dV_i):

$$q_i = Q_i - Q_{i-1} + \frac{dV_i}{V_o}\left(\frac{Q_i + Q_{i-1}}{2}\right) \qquad (5)$$

Fitting was performed with a Fortran-based program, written in-house. The integrated injection heats for each injection of Ca^{2+} are predicted by a two-step procedure. An iterative bisection routine furnishes estimates for the free Ca^{2+} and AB fragment concentrations, employing the relevant mass conservation relationships. These values are then substituted into eq 4 and 5 for calculation of the cumulative heat and heat of injection, respectively. The resulting χ^2 value is subjected to Marquardt−Levenberg minimization, employing the CURFIT algorithm from Bevington (*21*). During the fitting process, K_{11}, H_{11}, K_{21}, and H_{21} were allowed to vary. Starting estimates for these parameters were obtained by Monte Carlo analysis, as described elsewhere (*22*). K_{10} and H_{10} were fixed at 3600 M^{-1} and 2.1 kcal/mol, respectively, the values obtained from the previous analysis of Ca^{2+} binding to the isolated β CD-EF fragment (*18*).

The following discussion employs both microscopic (k_1, k_2) and macroscopic (K_1, K_2) Ca^{2+}-binding constants. The microscopic (or site-specific) constants, obtained with the independent two-site equation, reflect the affinities of discrete binding sites. By contrast, the macroscopic constants, obtained with the Adair analysis, reflect the average affinities associated with the two binding events. In the absence of positive cooperativity, the microscopic constants are related

to the macroscopic binding constants reported in Table 2 as follows:

$$K_1 = k_1 + k_2; \quad K_2 = k_1k_2/(k_1 + k_2) \tag{6}$$

$$k_1 = \frac{K_1 + \sqrt{K_1^2 - 4K_1K_2}}{2}; \quad k_2 = \frac{K_1 - \sqrt{K_1^2 - 4K_1K_2}}{2} \tag{7}$$

Circular dichroism measurements were conducted at 25 °C with an Aviv 62DS circular dichroism spectrometer in 0.1 cm cuvettes. Samples were prepared in 0.15 M NaCl and 0.005 M Hepes, pH 7.4, containing 0.001 M Ca^{2+}.

RESULTS

Sedimentation Equilibrium Analysis of the α and β AB Fragments. The propensities of the AB peptides to aggregate were examined by sedimentation equilibrium. The synthetic α AB fragment was loaded into the sample cell at nominal concentrations of 240, 120, and 60 μM and then centrifuged to equilibrium at 20 °C at a rotor speed of 40000 rpm, monitoring the absorbance at 257 nm. The resulting solute distributions, displayed in Figure 2A, are well accommodated by an ideal single-species model (eq 1). The best-fit estimate of the molecular weight is 4180 ± 150, in good agreement with the calculated monomer value of 4091.

Samples of synthetic β AB, at nominal concentrations of 840, 420, and 210 μM, were similarly analyzed. Because the β AB fragment contains a cysteine residue at position 18, it was dialyzed against buffer containing 1 mM TCEP prior to centrifugation to prevent disulfide bond formation. The higher concentration of this β AB solution permitted analysis with both absorbance (○) and interference optics (□). As shown in Figure 2B, the data for β AB can likewise be modeled with the assumption of a single species. The apparent molecular weight, 4140 ± 120, is in reasonable agreement with the predicted molecular weight for the synthetic peptide, 4043. Thus, the β AB fragment shows no significant tendency to self-associate in Hepes-buffered saline, pH 7.4, at 20 °C, even at concentrations approaching 1 mM.

Association of the AB and CD-EF Domains and Apparent Ca^{2+} Affinity of the Resulting Complexes. The following paragraphs examine the association reactions, both homologous and heterologous, between the AB and CD-EF fragments from rat α- and β-parvalbumin. The reactions were studied primarily by ITC. Two types of experiment are described. In one case, the CD-EF fragment was titrated with the AB fragment in the presence of saturating Ca^{2+}. In the second, an equimolar mixture of the two fragments was titrated with Ca^{2+} to evaluate the apparent Ca^{2+} affinity of the resulting AB/CD-EF complex. Thermodynamic data for the studies are summarized in Tables 1 and 2, respectively.

α AB and α CD-EF. An equimolar mixture of α AB and α CD-EF fragments was sedimented to equilibrium at rotor speeds of 25000 and 40000 rpm at 20 °C. When 1.0 mM EDTA was included in the sample (Figure 3A), the best fit to a single-species model yielded an average molecular weight of 5400 ± 200. By contrast, in the presence of 1.0 mM Ca^{2+}, this model returns a best-fit value of 10400 ± 200 (Figure 3B). The marked increase in average cell molecular weight suggests that association of the αAB and α CD-EF domains requires Ca^{2+}.

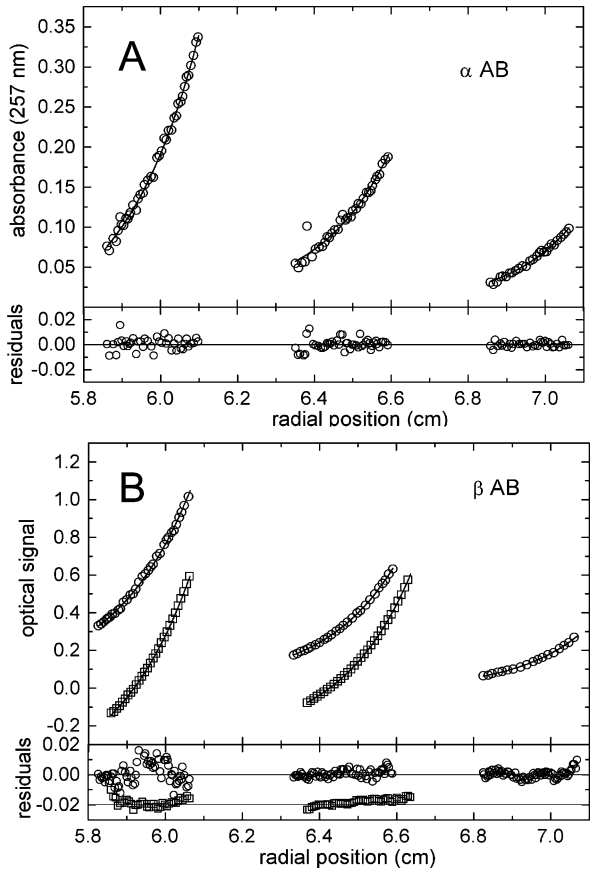

FIGURE 2: (A) Sedimentation equilibrium analysis of the rat α AB fragment. Samples of α AB (approximately 240, 120, and 60 μM) were centrifuged at 40000 rpm and 20 °C. The solid lines in the upper panel denote the best least-squares fit of the resulting data to an ideal single-species model. The corresponding residuals, observed minus calculated values, are displayed in the lower panel. For clarity, only a subset of the data is presented. (B) Sedimentation equilibrium analysis of the rat β AB fragment. Samples of β AB (approximately 840, 420, and 210 μM) were centrifuged to equilibrium at 40000 rpm and 20 °C. The peptide distributions were monitored by absorbance at 257 nm (○) and, at the two higher concentrations, by interference optics (□). The optical signal, absorbance or interference fringes, is plotted versus radial position. These five data sets were simultaneously fit to an ideal single-species model, the solid lines denoting the optimal fit. Residuals are displayed in the lower panel.

Table 1: Apparent Energetics of AB/CD-EF Complex Formation[a]

protein complex	K	ΔH	$\Delta G°$ [b]	$-T\Delta S$
α AB/α CD-EF	7.6 (0.4) × 10^6	−17.0 (0.1)	−9.3 (0.1)	7.7
β AB/α CD-EF	1.1 (0.6) × 10^6	−17.5 (0.2)	−8.2 (0.1)	4.4
recombinant β AB/β CD-EF	3.4 (0.2) × 10^6	−20.1 (0.1)	−8.9 (0.1)	11.2
synthetic β AB/β CD-EF	2.5 (0.1) × 10^6	−20.7 (0.1)	−8.7 (0.1)	12.0
α AB/β CD-EF	6.6 (0.4) × 10^6	−20.1 (0.1)	−9.3 (0.1)	10.8
pike AB/CD-EF[c]	2.2 × 10^5	nd	−7.3	nd

[a] Binding constants are expressed in M^{-1} and energies in kcal/mol. Uncertainties (68% confidence intervals) are listed in parentheses. All data were collected at 25 °C in 0.15 M NaCl and 0.025 M Hepes, pH 7.4, except those reported for the pike parvalbumin fragments. The latter were collected in 50 mM Tris-HCl, pH 7.5. [b] $\Delta G° = -RT \ln K$. [c] From ref *19*.

This conclusion is supported by ITC measurements of complex formation. Raw data for the titration of α CD-EF

Table 2: Apparent Ca^{2+}-Binding Energetics of the AB/CD-EF Complexes, Isolated CD-EF Fragments, and Intact Proteins[a]

protein/complex	K_1	ΔH_1	K_2	ΔH_2	ΔG_{tot}[b]	ΔH_{tot}	$-T\Delta S_{tot}$
rat α-PV[e]	2.5 (0.2) × 10^8	−1.3 (0.1)	6.2 (0.2) × 10^7	−4.3 (0.1)	−22.0	−5.6	−16.4
α CD-EF[f]	3.7 (0.1) × 10^3	−17.2 (0.2)	8.6 (0.2) × 10^4	−4.0 (0.3)	−11.6	−21.2	9.6
α CD-EF[g]	1.0 × 10^5	nd[c]	2.5 × 10^5	nd	−15.5	nd	nd
α AB/α CD-EF	1.7 (0.4) × 10^6	−22 (0.1)	4.3 (0.2) × 10^5	−22 (0.1)	−16.1	−44.0	27.9
β AB/α CD-EF	1.1 (0.1) × 10^5	−21.7 ± 0.7	1.5 (0.1) × 10^4	−2.0 ± 0.7	−12.5	−23.7	11.2
rat β-PV[e]	2.4 (0.2) × 10^7	−4.1 (0.1)	1.4 (0.2) × 10^6	−3.5 (0.1)	−18.4	−7.6	−10.8
β CD-EF[f]	4.2 (1.0) × 10^3	2.1 (0.2)	6.1 (1.9) × 10^3	−22.8 (1.5)	−10.1	−24.9	14.8
recombinant β AB/β CD-EF	1.1 (0.2) × 10^5	−26.6[d]	2.5 (0.2) × 10^4	−3.6	−12.7	−30.2	17.5
synthetic β AB/β CD-EF	1.0 (0.2) × 10^5	−28.1[d]	2.1 (0.2) × 10^4	−2.3	−12.7	−30.4	17.7
α AB/β CD-EF	1.3 (0.1) × 10^6	−17.5 (0.1)	8.8 (0.2) × 10^4	−16.3 (0.1)	−15.0	−33.8	18.8
pike PV[h]	4.0 (2.8) × 10^8	nd	6.3 (4.3) × 10^8	nd	−23.6	nd	nd
pike CD-EF[i]	1.2 (0.8) × 10^6	nd	1.0 (0.7) × 10^7	nd	−17.8	nd	nd
pike AB/CD-EF[i]	2.5 (1.7) × 10^7	nd	4.0 (2.8) × 10^8	nd	−21.7	nd	nd

[a] The macroscopic stepwise binding constants are expressed in $M^{-1}$and energies in kcal/mol. Uncertainties (68% confidence intervals) are listed in parentheses. Data were collected at 25 °C in 0.15 M NaCl and 0.025 M Hepes, pH 7.4, except those reported for pike parvalbumin and its fragments. The latter were collected in 50 mM Tris-HCl, pH 7.5. [b] Apparent total standard free energy, $\Delta G_{tot} = -RT \ln(K_1K_2)$. [c] Not determined. [d] These values represent the sum of the enthalpy changes for binding of the first Ca^{2+} ion and association of the AB and CD-EF fragments ($H_{10} + H_{11}$ in eq 4). [e] From ref *22*. [f] From ref *18*. [g] From ref *40*. [h] From ref *39*. [i] From ref *19*.

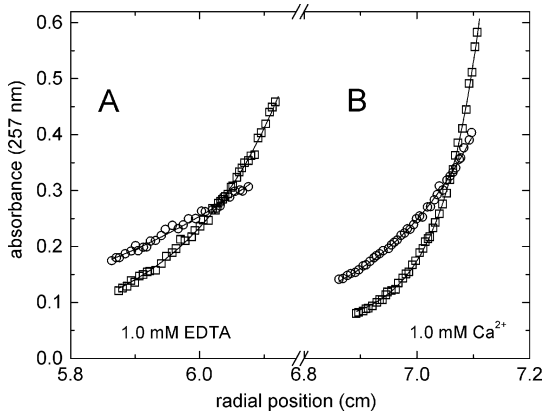

FIGURE 3: Sedimentation equilibrium analysis of a mixture of α AB and α CD-EF. An equimolar mixture of the peptides was centrifuged to equilibrium at 25000 (○) and 40000 (□) rpm, 20 °C, in buffer containing either 1.0 mM EDTA (A) or 1.0 mM Ca^{2+} (B). The resulting solute distributions were monitored by absorbance at 257 nm. These data were arbitrarily fit to a single-species model to extract an average cell molecular weight.

with α AB, in the presence of either 1.0 mM Ca^{2+} or 1.0 mM EDTA, are presented in Figure 4A. The heat effects observed in the presence of EDTA, vertically offset for clarity, are indistinguishable from those obtained by injection of the AB peptide into buffer. Thus, at the concentrations employed for ITC, the interaction between the AB and CD-EF fragments appears to be absolutely dependent upon Ca^{2+}.

Integrated data for the titration performed in the presence of saturating Ca^{2+} are shown in Figure 4B. Analysis with a single-site model yields an apparent K_a of 7.6 × 10^6 M^{-1}, corresponding to an apparent standard free energy change of −9.3 kcal/mol (Table 1). The reaction is enthalpically driven ($\Delta H = -17.0$ kcal/mol), and the associated standard entropy change is decidedly unfavorable ($-T\Delta S = 7.7$ kcal/mol).

When an approximately equimolar mixture of α AB and α CD-EF is titrated with Ca^{2+} (Figure 4C), the integrated data (Figure 4D, ○) can be treated with an identical two-site model. The average microscopic association constant for Ca^{2+} is 8.5 × 10^5 M^{-1}, and the reaction is strongly exothermic, with a total enthalpy change of −44 kcal/mol (Table 2). This behavior contrasts sharply with that observed in titrations of the isolated α CD-EF fragment, included in Figure 4D for comparison (□). Ca^{2+} binding in the latter case is positively cooperative, requiring application of a two-site Adair model for successful least-squares minimization (*18*). In this context, it should be noted that Table 2 lists apparent macroscopic Ca^{2+}-binding constants to facilitate comparison with experiments described below that cannot be satisfactorily analyzed with an independent two-site model.

β AB and α CD-EF. Relative to the behavior of α AB, the β AB fragment associates less tightly with α CD-EF. Raw data for a representative titration are presented in Figure 5A, and the corresponding integrated data are presented in Figure 5B. The apparent association constant for this reaction, conducted in 10 mM Ca^{2+}, is 1.1 × 10^6 M^{-1}, a factor of 6.9 smaller than that measured for the reaction between α AB and α CD-EF. At −17.5 kcal/mol, the apparent enthalpy of the reaction is comparable to that for α/α (−17 kcal/mol).

The Ca^{2+} affinity of the β AB/α CD-EF complex is substantially lower than that measured for α/α. Raw data for the titration of a mixture of the two fragments are displayed in Figure 5C. Whereas the two sites in the α/α complex behave equivalently when titrated with Ca^{2+}, the integrated β/α data (Figure 5D) require a nonidentical two-site model. The apparent microscopic Ca^{2+} association constants are 9.1 × 10^4 and 1.8 × 10^4 M^{-1}. The total binding enthalpy, −24 kcal/mol, is far less exothermic than that associated with Ca^{2+} binding by the α/α complex (−44 kcal/mol).

β AB and β CD-EF. A representative titration of the β CD-EF fragment with recombinant β AB is depicted in Figure 6, raw data in panel A and integrated data with least-squares fit in panel B (○). This experiment was conducted in the presence of 10 mM Ca^{2+}, rather than 1 mM, because β CD-EF has approximately 10-fold lower intrinsic affinity for Ca^{2+} than the corresponding α fragment (*18*). Under these conditions, the two fragments associate with an apparent binding constant of 3.4 × 10^6 M^{-1} and a binding enthalpy of −20.1 kcal/mol. Due to its pronounced tendency to self-associate in the Ca^{2+}-bound state, β CD-EF will be dimeric at the start of the titration, and formation of the AB/CD-EF complex will presumably require dissociation of the dimer.

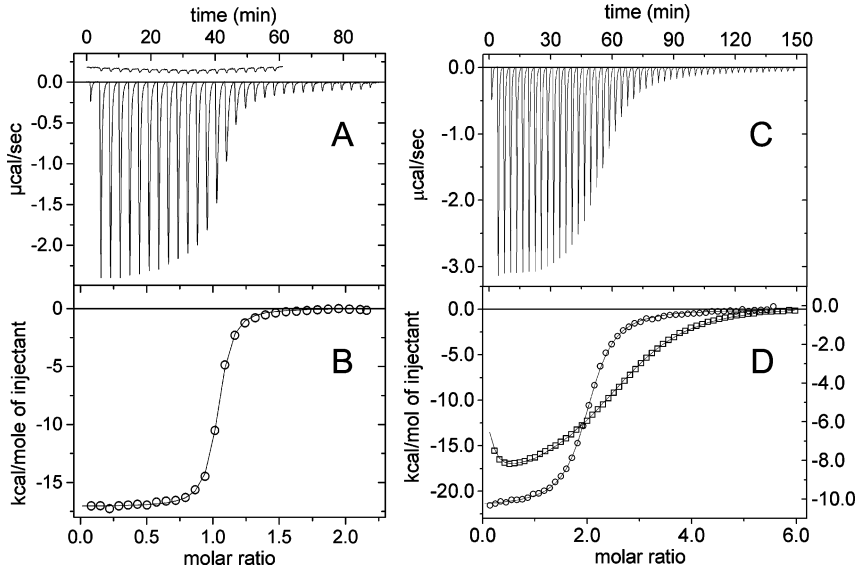

FIGURE 4: Calorimetric analysis of the interaction between α AB and α CD-EF. (A) Raw data for the titration of 48 μM α CD-EF with 0.46 mM α AB in Hepes-buffered saline, pH 7.4, containing 1.0 mM Ca^{2+}. Corresponding data for the same titration conducted in buffer containing 1.0 mM EDTA are also displayed, offset slightly for clarity. (B) Integrated data for the titration in panel A with the best fit to a single-site model. (C) Raw data for the titration of α AB (40 μM) and α CD-EF (35 μM) with Ca^{2+}. Excess AB was included to ensure that all of the CD-EF fragment could be complexed. (D) Integrated data for the titration presented in panel C (○) with the best least-squares fit to an identical two-site model. A titration of the isolated α CD-EF fragment is shown for comparison (□). The left and right axes pertain to the α/α complex and isolated α CD-EF fragment, respectively.

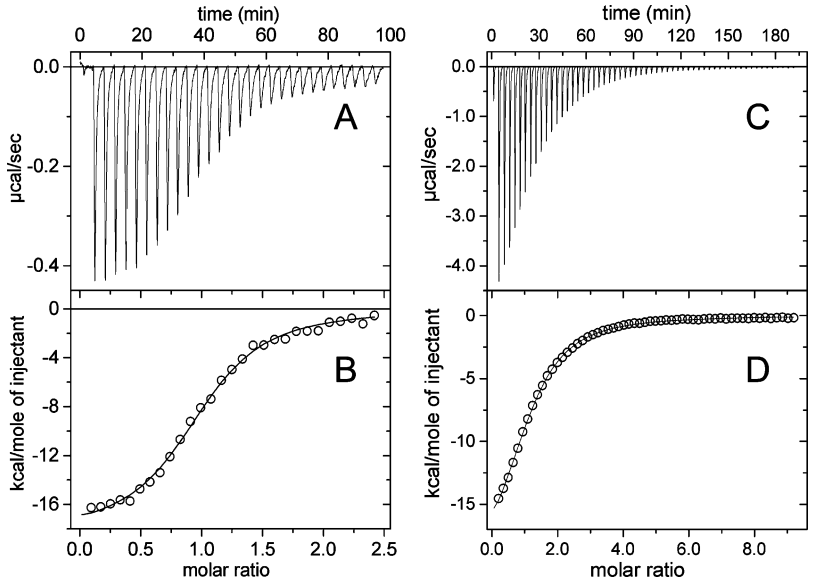

FIGURE 5: Analysis of the interaction between β AB and α CD-EF. (A) Raw data for the titration of 15 μM α CD-EF with 0.16 mM β AB in Hepes-buffered saline, pH 7.4, containing 10 mM Ca^{2+} and 1.0 mM DTT. (B) Integrated data for the titration shown in panel A with the best fit to a single-site model. (C) Raw data for the titration of β AB (50 μM) and α CD-EF (45 μM) with Ca^{2+} in Hepes-buffered saline plus 1.0 mM DTT. (D) Integrated data for the titration presented in panel C with the best fit to an independent two-site model.

Figure 6C displays raw data for the titration of a roughly equimolar mixture of recombinant β AB and β CD-EF fragments with Ca^{2+}. The corresponding integrated data are presented in Figure 6D (○). Qualitatively, they resemble those observed in titrations of the isolated β CD-EF fragment (■), although the Ca^{2+} affinity is higher for the AB/CD-EF mixture. Interestingly, the early points in the titration of the complex cannot be accommodated with a general two-site model. The best fit to a two-site Adair model (dashed line), clearly unsatisfactory, yields apparent macroscopic association constants of 2.9×10^5 and 2.3×10^4 M^{-1}. The appearance of these data suggested that the β AB fragment does not associate tightly with the half-saturated β CD-EF fragment; i.e., an equilibrium exists between CaCD-EF and CaAB/CD-EF during the titration. To examine this possibility, a model was employed (see Materials and Methods) that included these species in the partition function: CD-EF, CaCD-EF, CaAB/CD-EF, and Ca_2AB/CD-EF. For fitting, the binding constant and enthalpy for the first Ca^{2+}-binding event (K_{10} and H_{10} in eq 4) were fixed at the values obtained from the previous study of the isolated CD-EF domains (*18*). The adjustable parameters included the binding constant and enthalpy change for the association of β AB with CaCD-EF (K_{11} and H_{11}) and for binding of the second Ca^{2+} to the CaAB/CD-EF complex (K_{21} and H_{21}). The optimal values for these parameters are listed in Table 3. It is evident from

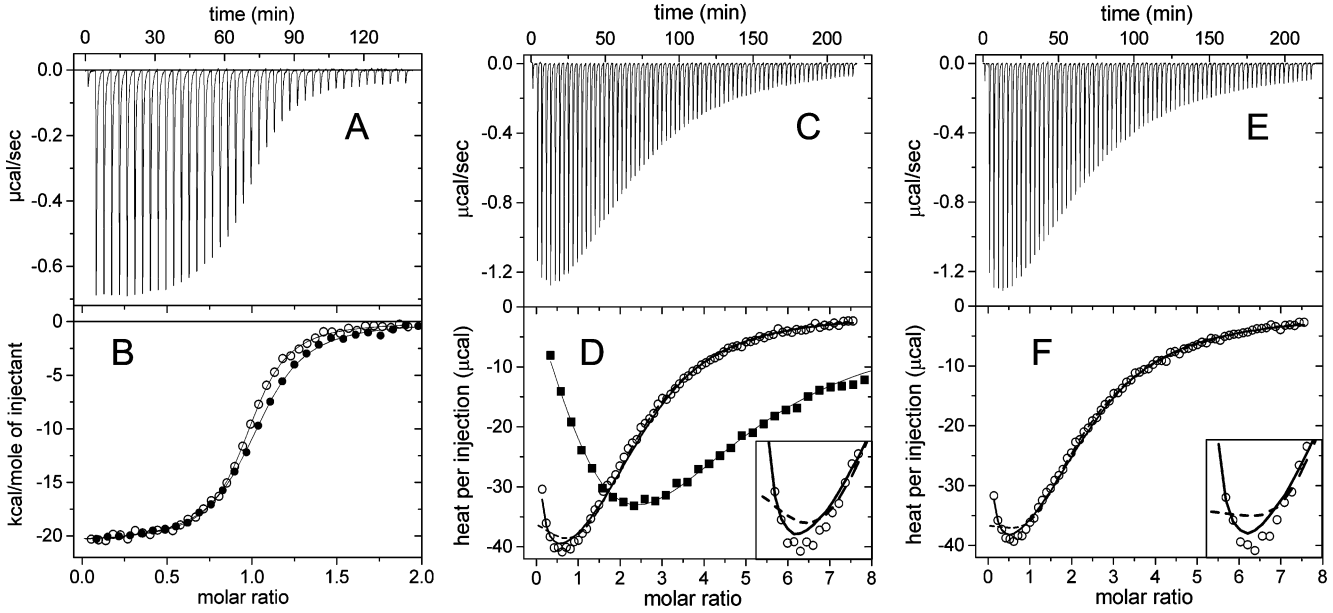

FIGURE 6: Analysis of the interaction between β AB and β CD-EF. (A) Raw data for the titration of 20 μM β CD-EF with 0.25 mM recombinant β AB in Hepes-buffered saline, pH 7.4, containing 10 mM Ca^{2+} and 1.0 mM DTT. (B) Integrated data for the titration shown in panel A are represented by the open circles (○). The solid circles (●) are data from a comparable experiment conducted with synthetic β AB (0.26 mM synthetic β AB vs 20 μM β CD-EF). (C) Raw data for the titration of recombinant β AB (35 μM) and β CD-EF (30 μM) with Ca^{2+}. (D) Integrated data for the titration in panel C (○), the best least-squares fit to a two-site Adair model (dashed line), and the best fit to the more complex model described in the text (solid line). Inset: early portion of the titration magnified to more clearly reveal the difference in the quality of the fit. The solid squares (■) are data from a titration of 60 μM β CD-EF alone with 4.0 mM Ca^{2+}. (E) Raw data for the titration of synthetic β AB (35 μM) and β CD-EF (30 μM) with Ca^{2+}. (F) Integrated data for the experiment in panel E (○), the best fit to a two-site Adair model (dashed line), and the best fit to the more complex model described in the text (solid line).

Table 3: Ca^{2+}-Binding Parameters for the β AB/β CD-EF Complex[a]

protein/complex	K_{10}[b]	H_{10}[b]	K_{11}	H_{11}	K_{21}	H_{21}
recombinant β AB	3.6 (0.3) × 10^3	2.1	5.5 (0.2) × 10^4	−28.7	5.9 (0.3) × 10^5	−3.6
synthetic β AB	3.6 (0.3) × 10^3	2.1	7.2 (0.3) × 10^4	−30.2	4.4 (0.3) × 10^5	−2.3

[a] The binding constants are expressed in M^{-1} and energies in kcal/mol. Uncertainties (68% confidence intervals) are listed in parentheses. [b] Fixed at the values determined in ref *18*.

Figure 6D that this model provides a better fit (solid line) than the Adair model to the early portion of the titration.

The binding constants afforded by this model were used to construct a Ca^{2+}-binding curve for this experiment (Figure 7A, ○). Estimates for the apparent Ca^{2+}-binding constants were obtained by taking the reciprocal of the free Ca^{2+} concentration at $\bar{X} = 0.5$ and $\bar{X} = 1.5$. This procedure yielded values of 1.1 × 10^5 and 2.5 × 10^4 M^{-1}, which have been included in Table 2. In this context, it should be noted that the ΔH_1 value entered in Table 2 for this reaction represents the sum of H_{10} and H_{11} in eq 4.

The derivative of the binding curve ($d\bar{X}/d\ln[Ca^{2+}]$) is plotted in Figure 7B (○). Whereas a maximum value of 0.5 is observed for noncooperative two-site binding (*23*), the derivative in the present case reaches a value of 0.66, indicative of positive cooperativity. The appearance of the binding curve for the AB fragment, also plotted in Figure 7A (●), is consistent with this conclusion. For example, when 1 equiv of Ca^{2+} has been bound, the fraction of CD-EF molecules complexed with AB is just 0.52. This result suggests that the preponderance of the AB/CD-EF complex is fully Ca^{2+} bound; i.e., Ca^{2+} binding is strongly cooperative.

The synthetic β AB fragment behaves similarly. When β CD-EF is titrated with synthetic AB, in the presence of saturating Ca^{2+}, the resulting integrated data (Figure 6B, ●) can be fit with an apparent binding enthalpy of −20.7 kcal/mol and an apparent binding constant of 2.5 × 10^6 M^{-1}. When a mixture of synthetic β AB and β CD-EF is titrated with Ca^{2+}, the resulting data (Figure 6F, ○) are likewise

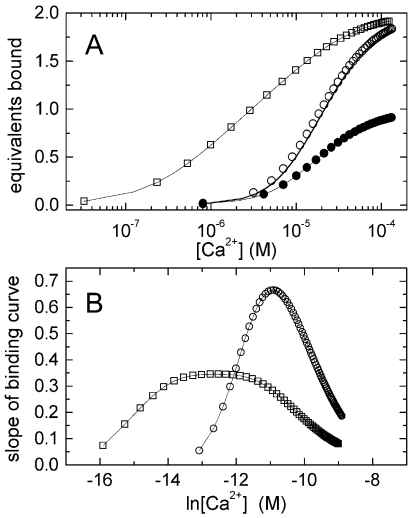

FIGURE 7: (A) Simulated Ca^{2+}-binding curves from Ca^{2+} titrations of recombinant β AB/β CD-EF (○) and synthetic β AB/β CD-EF (heavy solid line). The solid circles (●) reflect the associated binding of recombinant β AB to β CD-EF. The Ca^{2+}-binding curve from the titration of α/β (□) is also shown for comparison. (B) Derivative of the Ca^{2+}-binding curves for recombinant β/β (○) and α/β (□).

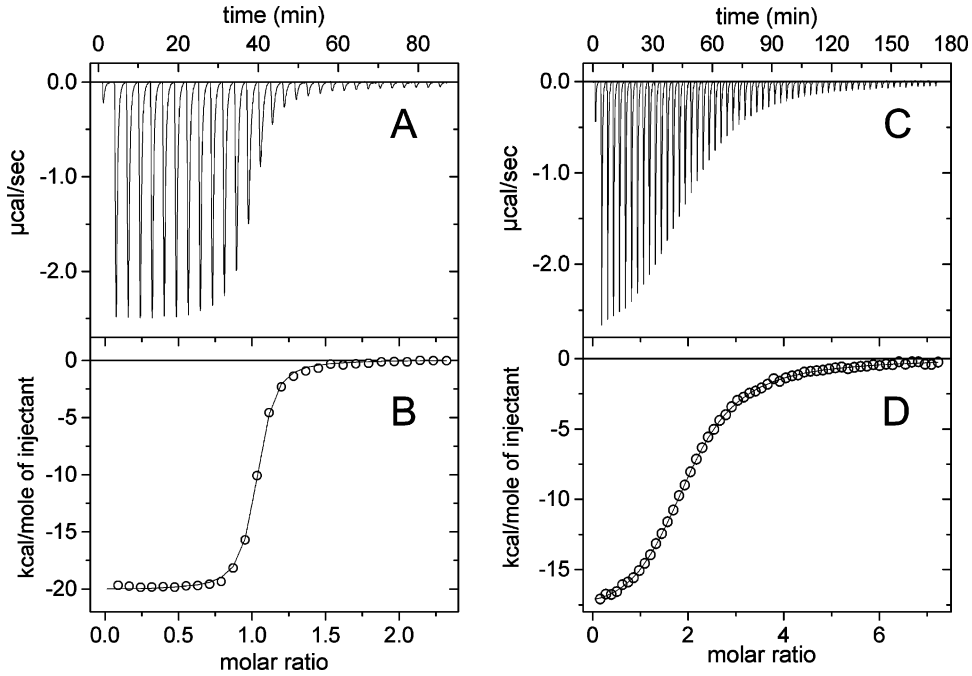

FIGURE 8: Analysis of the interaction between α AB and *β* CD-EF. (A) Raw data for the titration of 48 uM *β* CD-EF with 0.46 mM α AB at 25 °C in Hepes-buffered saline, pH 7.4, containing 10 mM Ca^{2+}. (B) Integrated data for the titration shown in panel with the best least-squares fit to a single-site model. (C) Raw data for the titration of a solution of α AB (40 *μ*M) and *β* CD-EF (30 *μ*M) with Ca^{2+}. (D) Integrated data for the titration presented in panel C with the best fit to an independent two-site model.

incompatible with a two-site Adair model (dashed line). Application of the more complex model discussed earlier affords binding constant and enthalpy estimates of 7.2×10^4 M^{-1} and −30.2 kcal/mol for the association of AB and CaCD-EF and 4.4×10^5 M^{-1} and −2.3 kcal/mol for binding of the second Ca^{2+} to the CaAB/CD-EF complex. A Ca^{2+}-binding curve for this experiment (Figure 7A, heavy solid line) was extracted from the titration data as described above. The apparent binding constants obtained from the curve were 1.0×10^5 and 2.1×10^4 M^{-1}.

α *AB and β CD-EF*. A representative titration of *β* CD-EF with the α AB fragment, in 10 mM Ca^{2+}, is displayed in Figure 8A,B. Interestingly, under these conditions, the *β* CD-EF fragment exhibits higher affinity for the α AB domain than for the *β* AB domain, either synthetic or recombinant. Whereas the association constant for the homologous complex is between 2.5×10^6 M^{-1} (synthetic *β* AB) and 3.4×10^6 (recombinant *β* AB), the corresponding value for the heterologous complex is 6.6×10^6 M^{-1}. The enthalpy of formation for the α/*β* complex is −20.1 kcal/mol, comparable to the value measured for *β*/*β* (−20.7 kcal/mol with synthetic *β* AB, −20.1 kcal/mol with recombinant *β* AB).

Consistent with the larger complex formation constant, the Ca^{2+} affinity of the αAB/*β* CD-EF complex is substantially greater than that displayed by the homologous *β* complex. The raw data obtained by titration of an equimolar α/*β* mixture with Ca^{2+} (Figure 8C) differ strikingly from those obtained with *β*/*β*. In contrast to the latter, the integrated data for the heterologous complex (Figure 8D) can be satisfactorily modeled with an independent two-site model. This finding implies that the half-saturated *β* CD-EF species has significantly higher affinity for the heterologous α AB fragment than for the homologous *β* AB fragment, so that the concentration of CaCD-EF present during the experiment is negligible. The apparent macroscopic Ca^{2+}-binding constants, 1.3×10^6 and 8.8×10^4 M^{-1}, are substantially larger than the estimates obtained for the *β*/*β* complex, and the total binding enthalpy, −33.8 kcal/mol, is 3.4−3.6 kcal/mol more exothermic. The Ca^{2+}-binding curve extracted from this experiment is displayed in Figure 7A (□). The displacement to lower Ca^{2+} concentrations emphasizes the increase in Ca^{2+} affinity, relative to *β*/*β*, and the greater breadth indicates the absence of positive macroscopic cooperativity. Consistent with that diagnosis, the slope of the α/*β* Ca^{2+}-binding curve (Figure 7B, □) does not exceed 0.35.

DISCUSSION

Transient increases in cytosolic Ca^{2+} reflect the coordinate action of pumps, channels, and Ca^{2+}-binding proteins. Thus, an appreciation of metal ion−protein interactions is essential for understanding Ca^{2+} signaling pathways. The mammalian parvalbumins offer an interesting system for exploring structure−function relationships in Ca^{2+}-binding proteins. Despite 49% sequence identity with rat α, the $\Delta G°'$ for Ca^{2+} binding is 3.6 kcal/mol less favorable for rat *β* in Hepes-buffered NaCl (*16*, *17*, *22*). An explanation for the disparate behavior of α and *β* could provide insight into the modulation of divalent ion affinity. Additionally, although both proteins presumably function as Ca^{2+} buffers, their expression patterns differ markedly. α is widely distributed. Particularly abundant in fast-twitch skeletal muscle, it is also expressed in an assortment of other cell types, notably rapidly firing neurons (*24*−*26*) and the *inner hair cells* of the mammalian auditory organ, or organ of Corti (*27*). The distribution of *β* is much more limited, with expression in postnatal mammals apparently restricted to the *outer hair cells* of the organ of Corti (*28*, *29*). The selective recruitment of α and *β* by the two sensory cell types in the auditory organ is intriguing. A thorough exposition of their divalent ion-binding properties, kinetic and thermodynamic, may help to resolve this enigma.

There is evidence that the attenuated divalent ion affinity of rat β is largely due to higher order structural considerations. Specifically, mutations at positions of nonidentity within the low-affinity CD binding loop of rat β have a modest impact on Ca^{2+} affinity (*16*, *30*, *31*). For example, the sequences of rat α and β differ at position 59, glutamate in α and aspartate in β. Although the replacement of one acidic side chain by another appears reasonably conservative, residue 59 contributes the $-x$ CD-site ligand. Whereas the glutamyl carboxylate can directly coordinate the bound Ca^{2+}, the shorter aspartyl side chain must coordinate indirectly, hydrogen bonding to a water molecule that serves as the proximal ligand. Prior to the detailed characterization of rat β, the glutamate $\rightarrow$ aspartate substitution was considered a primary reason for the reduced divalent ion affinity (*32*). Contrary to expectation, however, replacement of Asp-59 by glutamate produces an insignificant increase in the CD site Ca^{2+} affinity, improving the standard free energy for Ca^{2+} binding by 0.1 kcal/mol (*16*).

Interestingly, the reverse mutation (E59D) in rat α causes a substantial loss of affinity. The macroscopic Ca^{2+}-binding constants decrease from 2.5×10^8 and 6.2×10^7 M^{-1} to 1.2×10^8 and 7.9×10^6 M^{-1} (*33*), an apparent $\Delta\Delta G°'$ of 1.7 kcal/mol. This finding has major implications. Although the identity of the $-x$ ligand is a potentially critical determinant of affinity, the environment of the β CD site can evidently suppress its influence. In this context, the high-affinity EF site ligand array acquires a low-affinity signature when introduced into the rat β CD binding loop (*34*), likewise implying that the surrounding protein architecture perturbs the intrinsic behavior of the CD site ligand array.

NMR data suggest that the attenuation of rat β divalent ion affinity reflects, in part, antagonism between the β AB and CD-EF domains. The backbone dynamics of rat β were examined by ^{15}N relaxation, in both the Ca^{2+}-bound and Ca^{2+}-free states (*35*). Paradoxically, the order parameters for the AB and D/E regions of the molecule are generally higher in the Ca^{2+}-free state. This finding suggests that Ca^{2+} binding may provoke a significant conformational change in the N-terminal domain, the energetic cost of which could produce a net reduction in the Ca^{2+}-binding free energy.

To test this hypothesis, the energetics of the AB/CD-EF interaction have been examined, employing the isolated fragments from rat α and β. This approach was used previously to study association of the AB and CD-EF domains from pike parvalbumin III, an α isoform (*19*).

Prior to studying the AB/CD-EF interactions in rat α and β, the isolated CD-EF fragments from both proteins were characterized (*18*). Although the relative Ca^{2+} affinities of the α- and β CD-EF fragments qualitatively parallel those of the intact proteins, the disparity in standard binding free energy in Hepes-buffered saline is smaller for the fragments (1.5 vs 3.6 kcal/mol). This finding was viewed as consistent with a role for the AB domain in regulating divalent ion affinity. Although the intact proteins are strictly monomeric, the α and β CD-EF fragments exhibit some tendency to self-associate, and despite its higher net charge, Ca^{2+}-bound β CD-EF dimerizes far more readily than α CD-EF. Circular dichroism measurements suggest that the apo fragments are largely disordered. However, Ca^{2+}-free β CD-EF retains the capacity to dimerize weakly, suggesting that the folded state may be populated to some extent at 20 °C.

As observed with the pike PV fragments (*19*), formation of the rat AB/CD-EF complexes requires Ca^{2+}. The Ca^{2+} dependence is evident in both sedimentation (Figure 3) and ITC (Figure 4A) analyses. Besides the loss of translational/rotational entropy, AB/CD-EF complex formation is accompanied by a major reduction in conformational entropy because the unliganded CD-EF fragments are disordered (*18*). Presumably, the energetic gain of complex formation cannot offset this large entropic cost. However, Ca^{2+} binding promotes folding of the CD-EF fragment. Thus, in the presence of Ca^{2+}, the driving force for the AB/CD-EF interaction need only overcome the unfavorable entropy of AB organization, making the reaction energetically feasible.

The Ca^{2+} requirement for complex formation means that the apparent association constant is dependent on the free Ca^{2+} concentration and, conversely, that the apparent Ca^{2+}-binding constants are dependent on the fragment concentrations. To facilitate comparison between the various reactions, the association constants for AB/CD-EF complex formation were measured at saturating Ca^{2+} levels, i.e., saturating with respect to the isolated CD-EF fragments, and the Ca^{2+}-binding affinities were measured at similar concentrations of the AB and CD-EF fragments.

In the presence of saturating Ca^{2+}, complex formation can be viewed as a two-step process involving (a) isomerization of the AB fragment and (b) subsequent combination with Ca^{2+}-bound CD-EF:

$$AB_u \leftrightarrow AB_c; \quad \Delta H_{ab} \tag{8}$$

$$AB_c + Ca_2CD\text{-}EF \leftrightarrow Ca_2AB/CD\text{-}EF; \quad \Delta H_{com} \tag{9}$$

$$(Ca_2CD\text{-}EF)_2 \leftrightarrow 2Ca_2CD\text{-}EF; \quad -\Delta H_{dim} \tag{10}$$

In eqs 8 and 9, AB_u and AB_c represent the unliganded and complexed conformations of the AB fragment. ΔH_{ab} and ΔH_{com} symbolize the enthalpy changes for the AB isomerization and complexation reactions, respectively. The overall enthalpy change will equal $\Delta H_{ab} + \Delta H_{com}$. Because Ca^{2+}-bound β CD-EF is dimeric, the AB/CD-EF complexation reactions for β CD-EF will include dimer dissociation (eq 10), with its accompanying enthalpic contribution. The overall enthalpy change in this case will equal $\Delta H_{ab} + \Delta H_{com} - \Delta H_{dim}$.

Conceptually, the titration of a mixture of AB and CD-EF fragments with Ca^{2+} involves (a) isomerization of the AB fragment, (b) isomerization of CD-EF, (c) Ca^{2+} binding to the folded CD-EF fragment, and (d) formation of the Ca^{2+}-bound AB/CD-EF complex. Thus, in addition to eqs 8 and 9, this process also includes

$$CD\text{-}EF_u \leftrightarrow CD\text{-}EF_{ca}; \quad \Delta H_{cdef} \tag{11}$$

$$2Ca^{2+} + CD\text{-}EF_{ca} \leftrightarrow Ca_2CD\text{-}EF; \quad \Delta H_{Ca} \tag{12}$$

$CD\text{-}EF_u$ represents the disordered, apo form of the CD-EF fragment; $CD\text{-}EF_{ca}$ represents the form of the fragment competent to bind Ca^{2+}. The enthalpy change for the overall reaction should equal $\Delta H_{ab} + \Delta H_{cdef} + \Delta H_{com} + \Delta H_{Ca}$. Because the tendency for Ca^{2+}-free β CD-EF to dimerize is weak, its involvement here can be neglected.

In the following paragraphs, we discuss the energetics of complex formation at saturating Ca^{2+} levels and then focus

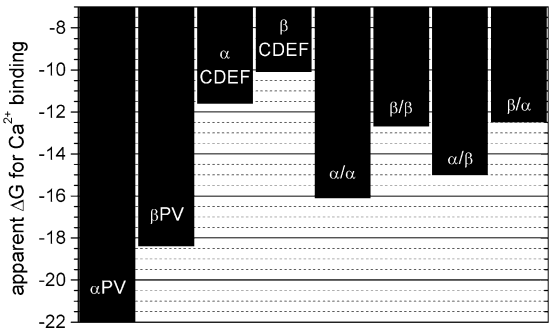

FIGURE 9: Apparent standard free energies of Ca^{2+} binding for the intact rat α- and *β*-parvalbumins, for the corresponding CD-EF fragments, and for the homologous and heterologous AB/CD-EF complexes.

attention on the apparent Ca^{2+} affinities. The differences in the standard free energy terms for the Ca^{2+}-binding reactions, depicted in Figure 9, offer some insight into the disparate divalent ion affinities of the two mammalian parvalbumins.

Association of the AB Domain with the Homologous Ca^{2+}-Bound CD-EF Domain. At saturating Ca^{2+} levels, the formation constant for the α/α complex is larger than that for *β*/*β*, 7.6×10^6 M^{-1} vs approximately 3.0×10^6 M^{-1}. (For clarity, the average values for the *β*/*β* system are employed throughout this discussion.) The lower affinity measured for *β*/*β* ($\Delta\Delta G \approx 0.6$ kcal/mol) may reflect, in part, the tendency for the Ca^{2+}-bound *β* CD-EF fragment to dimerize. Although structural data for the *β* CD-EF dimer are not available, it is likely that the self-association reaction juxtaposes the hydrophobic surfaces of two CD-EF fragments, reducing their accessibility for complexation with the AB fragment. If so, then formation of the Ca^{2+}-bound dimer, $(Ca_2CD\text{-}EF)_2$, would compete with formation of the Ca_2AB/CD-EF complex.

β/*β* association is apparently more exothermic than α/α. However, the *β* CD-EF dimerization reaction is endothermic, $\Delta H_{dim} = 5.6$ kcal/mol of dimer (*18*). Thus, the obligatory dissociation of the Ca^{2+}-bound dimer that must precede AB/CD-EF complex formation should contribute −2.8 kcal/mol to the apparent exothermicity of the AB/CD-EF complex formation. After correction for this phenomenon, the remainder (−17.6 kcal/mol), equal to the sum of $\Delta H_{ab} + \Delta H_{com}$, is comparable to that measured for α/α.

The apparent association constants determined for the rat α/α and *β*/*β* complexes are substantially higher than that reported (*19*) for the pike III AB/CD-EF complex (2.2×10^5 M^{-1}). However, the latter value was measured at a subsaturating Ca^{2+} concentration.

Association of the AB Domain with the Heterologous Ca^{2+}-Bound CD-EF Domain. The sequences of the α and *β* AB domains differ at 18 of 37 positions. Nevertheless, the *β* CD-EF domain associates more tightly with α AB than with the homologous AB fragment at saturating Ca^{2+} levels. Whereas the association constant for the *β*/*β* interaction is 3.0×10^6 M^{-1}, the corresponding value for α/*β* is 6.6×10^6 M^{-1} ($\Delta\Delta G \approx 0.5$ kcal/mol). The apparent enthalpies of complex formation, −20.4 (average) and −20.1 kcal/mol, respectively, are essentially identical. As discussed above for the *β*/*β* reaction, the overall enthalpy of complex formation includes an estimated −2.8 kcal/mol, due to dissociation of the Ca^{2+}-bound *β* CD-EF dimer. Thus, the corrected enthalpy of α/*β* complex formation would be approximately −17.3 kcal/mol.

The heightened affinity observed for the α/*β* complex is not general. The other heterologous interaction, i.e., between *β* AB and α CD-EF, is substantially weaker than the homologous α/α interaction in the presence of saturating Ca^{2+}. Thus, the preference of the *β* CD-EF fragment for the α AB domain suggests that some aspect of the *β* AB/*β* CD-EF complex formation is energetically unfavorable.

Ca^{2+} Affinities of the Homologous AB/CD-EF Complexes. The Ca^{2+}-binding behavior observed for an equimolar mixture of the α AB and α CD-EF fragments can be readily fit to an identical two-site model, yielding an overall standard free energy change of −16.1 kcal/mol. By contrast, the behavior of the *β*/*β* complex qualitatively resembles that observed for the isolated *β* CD-EF fragment, with the heat effects becoming increasingly exothermic at low Ca^{2+}:protein ratios and then gradually decreasing in magnitude. In contrast to the experiments conducted with α/α, *β*/α, and α/*β* mixtures, titrations of *β*/*β* with Ca^{2+} cannot be satisfactorily treated with a general two-site model. The inadequacy of the Adair model suggests that the *β* AB fragment does not associate tightly with the singly bound *β* CD-EF species, so that the CaCD-EF species is significantly populated during the course of the titration. Consistent with this hypothesis, a model that explicitly includes the CaCD-EF species yields a satisfactory fit, yielding an apparent standard free energy change of −12.7 kcal/mol.

Thus, when examined at similar peptide concentrations, the apparent standard free energy for binding of Ca^{2+} by the α/α complex is 3.4 kcal/mol more favorable than that measured for the *β*/*β* complex. This value approaches the 3.6 kcal/mol difference in standard binding free energy observed for the intact proteins (*23*). By contrast, the free energy difference measured for the isolated α and *β* CD-EF fragments is only 1.5 kcal/mol (*18*), implying that the presence of the AB domain magnifies the disparity in divalent ion-binding behavior.

As noted earlier, after correction for dimer dissociation, the enthalpy of *β*/*β* complex formation is comparable to that of α/α in the presence of saturating Ca^{2+}. In sharp contrast, the apparent total enthalpy of Ca^{2+} binding is far more exothermic for α/α than for *β*/*β* (−44 vs −30.3 kcal/mol). As discussed above, the reaction enthalpy in the latter case includes contributions from Ca^{2+} binding (ΔH_{Ca}) and from conformational reorganization of the CD-EF domain (ΔH_{cdef}). The enthalpy of Ca^{2+} binding is unlikely to be the source of the difference observed here, given the similarity in Ca^{2+} ligation observed for the α- and *β*-parvalbumins. More likely, the discrepancy reflects a difference in the ΔH_{cdef} terms for the α and *β* CD-EF fragments. Consistent with this hypothesis, the Ca^{2+}-binding enthalpy for the α/*β* complex is similarly reduced.

In the study of the isolated α and *β* CD-EF fragments (*18*), neither fragment displayed a cooperative denaturation transition in the Ca^{2+}-free state. However, the weak tendency for Ca^{2+}-free *β* CD-EF, but not α CD-EF, to dimerize suggests that the *β* fragment may retain more residual structure than α in the apo form. Resultingly, Ca^{2+} binding by *β*/*β* might be accompanied by a smaller enthalpy of folding. Alternatively, the disparate ΔH_{cdef} values may reflect a difference in the protonation equilibria that accompany folding of the two CD-EF fragments. The enthalpy of protonation of Hepes is considerable, −5.1 kcal/mol (*36*).

Thus, the release of two to three additional protons by the α CD-EF fragment during folding could account for the apparent difference in reaction enthalpy. To date, the buffer dependence of the apparent enthalpy changes has not been investigated.

The Ca^{2+}-binding constants reported for the pike III AB/CD-EF complex, and for the isolated pike CD-EF fragment as well, are substantially larger than those measured for the rat α/α and *β*/*β* complexes. Whereas the data reported here were collected in 0.15 M NaCl and 0.025 M Hepes, pH 7.4, the measurements on the pike system were conducted in 50 mM Tris-HCl, pH 7.5. Na^+ can seriously impact parvalbumin Ca^{2+} affinity by competing with the divalent ion for one or both vacant EF-hand motifs (*37*). For example, the rat α Ca^{2+}-binding constants are an order of magnitude larger in K^+ solution (*22*). The absence of Na^+ and the lower ionic strength in the pike PV experiments would both tend to promote divalent ion binding and could account for the higher Ca^{2+} affinities reported for that system.

Ca^{2+} Affinity of the Heterologous AB/CD-EF Complexes. In contrast to the corresponding experiments on *β*/*β*, Ca^{2+} titrations of α/*β* bear no qualitative resemblance to those performed with the isolated *β* CD-EF domain. Instead, the data can be treated with an independent, two-site model. The interaction of the α AB fragment with the half-saturated *β* CD-EF fragment must be sufficiently favorable that the concentration of CaCD-EF present during the titration is negligible. Evidently, relative to *β* AB, a smaller fraction of the intrinsic binding free energy associated with the first Ca^{2+}-binding event is required to promote association with the α AB fragment. This conclusion lends additional support to the hypothesis that Ca^{2+} binding by the intact *β*-parvalbumin is opposed by a conformational rearrangement of the AB domain.

The Ca^{2+} affinity measured for the heterologous α/*β* complex is 2.3 kcal/mol more favorable than that measured for the homologous *β*/*β* complex. The estimated $\Delta\Delta H_{Ca}$ value ($\Delta H_{\alpha\beta} - \Delta H_{\beta\beta}$) is −3.5 kcal/mol, indicating that the improvement in ΔG has an enthalpic origin. Because the contacting surfaces of α AB and *β* CD-EF should not exhibit optimal complementarity, it is unlikely that the *β* CD-EF fragment would associate more effectively with the heterologous α AB fragment than with its homologous partner domain.

Alternatively, the increased exothermicity of Ca^{2+} binding by α/*β* value may reflect a difference in the conformational reorganization terms for the α and *β* AB domains. As described in Materials and Methods, it was not possible to isolate full-length recombinant α AB. Mass spectrometric analysis of the purified material revealed a mixture of species consistent with proteolytic cleavage between residues 21−25. By contrast, the purified recombinant *β* AB was isolated intact, with no evidence of truncated contaminants. This disparate behavior suggests that free *β* AB adopts a defined tertiary structure, whereas α AB does not. If the conformation of the *β* AB fragment differs in the free and complexed state, then association of *β* AB with *β* CD-EF will require disruption of intradomain noncovalent contacts. Thus, Ca^{2+}-promoted complexation of *β* AB and *β* CD-EF may be subject to an additional enthalpic surcharge not incurred in the corresponding reaction between the (disordered) α AB fragment and *β* CD-EF.

The apparent entropic contributions to the Ca^{2+}-binding reactions support this interpretation. The $-T\Delta S$ term is 1.2 kcal/mol less favorable for the α/*β* reaction, consistent with the hypothesis that the α AB fragment is less structured than *β* AB prior to complex formation. In this context, previous site-specific mutagenesis data from this laboratory traced the atypical stability of Ca^{2+}-free rat *β* to the presence of proline at positions 21 and 26 (*38*). The analysis of the *β* P21A and *β* P26A variants indicated that Pro-21 and Pro-26 produce, as expected, a marked reduction in conformational entropy. This phenomenon may contribute to the proposed ability of *β* AB, but not α AB, to adopt a compact structure.

The impact of the α AB fragment on the Ca^{2+}-binding behavior of *β* CD-EF is not reciprocal. In the presence of the *β* AB fragment, the Ca^{2+} titration of the α CD-EF fragment (Figure 4D, □) no longer exhibits the cooperativity observed in titrations of the isolated CD-EF fragment (Figure 4D, □), and the data can be treated with an independent two-site model. However, the apparent Ca^{2+} affinity of the *β*/α complex is increased by just 0.9 kcal/mol.

CONCLUDING REMARKS

This study has examined the interaction between the parvalbumin AB and CD-EF domains, using the rat α and *β* fragments. Data were collected for the homologous (α/α, *β*/*β*) and heterologous (*β*/α, α/*β*) complexes, measuring the $\Delta G^{\circ\prime}$ for association in saturating Ca^{2+} and the apparent Ca^{2+} affinity at an arbitrary concentration of the complex.

Contrasts between the four complexes are muted at high Ca^{2+} levels, with the $\Delta G^{\circ\prime}$ values for complexation spanning just 1.1 kcal/mol. The data nevertheless suggest that the *β* AB fragment associates less avidly with the CD-EF fragments.

The differences become more obvious when the apparent Ca^{2+} affinities are compared. In a previous study on the isolated CD-EF fragments, the $\Delta\Delta G_{Ca}$ value ($\Delta G_{\alpha} - \Delta G_{\beta}$) was −1.5 kcal/mol. In the presence of the homologous AB fragment, the overall $\Delta\Delta G_{Ca}$ value shifts to −3.4 kcal/mol. The latter value approaches the $\Delta\Delta G_{Ca}$ value of −3.6 kcal/mol measured for the intact proteins in Hepes-buffered saline. The AB fragment evidently amplifies the difference in Ca^{2+} affinity observed for the two mammalian parvalbumin CD-EF domains.

However, the α and *β* AB domains differ with respect to their impact on CD-EF Ca^{2+} affinity. In the presence of α AB, the apparent Ca^{2+} affinities of α CD-EF and *β* CD-EF improve by 4.5 and 4.9 kcal/mol, respectively. In the presence of the *β* AB, however, the improvements are just 0.9 and 2.6 kcal/mol, respectively. These results imply that the *β* AB fragment is less effective than α AB at promoting Ca^{2+} chelation by the CD-EF fragment.

The basis for the disparate impact of α and *β* AB is conjectural. Interestingly, whereas α AB is highly susceptible to proteolysis, *β* AB is not. This observation suggests that the latter, but not the former, possesses a defined tertiary structure. Consistent with that idea, Ca^{2+} binding is less exothermic for *β*/*β* than for α/*β*. A significant energetic cost for conformational rearrangement could explain the smaller net gain in Ca^{2+} affinity. In closing, it is evident that parvalbumin Ca^{2+} affinity can be modulated by the interaction between the AB and CD-EF domains. Allosteric

phenomena are among the more intriguing aspects of protein/enzyme action. The parvalbumin molecule, with its juxtaposition of a single EF-hand domain and an autonomous structural element, may offer a useful model system for examining the influence of remote determinants on ligand-binding events.

REFERENCES

1. Kretsinger, R. H. (1980) Structure and evolution of calcium modulated proteins, *CRC Crit. Rev. Biochem. 8*, 115−164.
2. Kawasaki, H., and Kretsinger, R. H. (1994) Calcium-binding proteins 1: EF-hands, *Protein Profile 1*, 343−517.
3. Celio, M. R., Pauls, T., and Schwaller, B. (1996) *Guidebook to the Calcium-Binding Proteins*, Oxford University Press, New York.
4. McPhalen, C. A., Strynadka, N. C., and James, M. N. (1991) Calcium-binding sites in proteins: a structural perspective, *Adv. Protein Chem. 42*, 77−144.
5. Falke, J. J., Drake, S. K., Hazard, A. L., and Peersen, O. B. (1994) Molecular tuning of ion binding to calcium signaling proteins, *Q. Rev. Biophys. 27*, 219−290.
6. Linse, S., and Forsen, S. (1995) Determinants that govern high-affinity calcium binding, *Adv. Second Messenger Phosphoprotein Res. 30*, 89−151.
7. Declercq, J. P., Tinant, B., Parello, J., and Rambaud, J. (1991) Ionic interactions with parvalbumins. Crystal structure determination of pike 4.10 parvalbumin in four different ionic environments, *J. Mol. Biol. 220*, 1017−1039.
8. Wnuk, W., Cox, J. A., and Stein, E. A. (1982) Parvalbumins and other soluble high-affinity calcium-binding proteins from muscle, *Calcium Cell Funct. 2*, 243−278.
9. Pauls, T. L., Cox, J. A., and Berchtold, M. W. (1996) The Ca^{2+}-binding proteins parvalbumin and oncomodulin and their genes: new structural and functional findings, *Biochim. Biophys. Acta 1306*, 39−54.
10. Ahmed, F. R., Rose, D. R., Evans, S. V., Pippy, M. E., and To, R. (1993) Refinement of recombinant oncomodulin at 1.30 Å resolution, *J. Mol. Biol. 230*, 1216−1224.
11. Kretsinger, R. H., and Nockolds, C. E. (1973) Carp muscle calcium-binding protein. II. Structure determination and general description, *J. Biol. Chem. 248*, 3313−3326.
12. Epstein, P., Means, A. R., and Berchtold, M. W. (1986) Isolation of a rat parvalbumin gene and full length cDNA, *J. Biol. Chem. 261*, 5886−5891.
13. Gillen, M. F., Banville, D., Rutledge, R. G., Narang, S., Seligy, V. L., Whitfield, J. F., and MacManus, J. P. (1987) A complete complementary DNA for the oncodevelopmental calcium-binding protein, oncomodulin, *J. Biol. Chem. 262*, 5308−5312.
14. Pauls, T. L., Durussel, I., Cox, J. A., Clark, I. D., Szabo, A. G., Gagne, S. M., Sykes, B. D., and Berchtold, M. W. (1993) Metal binding properties of recombinant rat parvalbumin wild-type and F102W mutant, *J. Biol. Chem. 268*, 20897−20903.
15. Eberhard, M., and Erne, P. (1994) Calcium and magnesium binding to rat parvalbumin, *Eur. J. Biochem. 222*, 21−26.
16. Hapak, R. C., Lammers, P. J., Palmisano, W. A., Birnbaum, E. R., and Henzl, M. T. (1989) Site-specific substitution of glutamate for aspartate at position 59 of rat oncomodulin, *J. Biol. Chem. 264*, 18751−18760.
17. Cox, J. A., Milos, M., and MacManus, J. P. (1990) Calcium- and magnesium-binding properties of oncomodulin, *J. Biol. Chem. 265*, 6633−6637.
18. Henzl, M. T., Agah, S., and Larson, J. D. (2003) Characterization of the metal ion-binding domains from rat α- and β-parvalbumins, *Biochemistry 42*, 3594−3607.
19. Permyakov, E. A., Medvedkin, V. N., Mitin, Y. V., and Kretsinger, R. H. (1991) Noncovalent complex between domain AB and domains CD*EF of parvalbumin, *Biochim. Biophys. Acta 1076*, 67−70.
20. Cantor, C. R., and Schimmel, P. R. (1980) *Biophysical Chemistry II. Techniques for the study of biological structure and function*, p 624, W. H. Freeman and Co., San Francisco.
21. Bevington, P. R. (1969) Data reduction and error analysis for the physical sciences, McGraw-Hill, Boston.
22. Henzl, M. T., Larson, J. D., and Agah, S. (2004) Influence of monovalent cation identity on parvalbumin divalent ion-binding properties, *Biochemistry 43*, 2747−2763.
23. Wyman, J., and Gill, S. J. (1990) *Binding and Linkage*, University Science Books, Mill Valley, CA.
24. Muntener, M., Kaser, L., Weber, J., and Berchtold, M. W. (1995) Increase of skeletal muscle relaxation speed by direct injection of parvalbumin cDNA, *Proc. Natl. Acad. Sci. U.S.A. 92*, 6504−6508.
25. Schwaller, B., Dick, J., Dhoot, G., Carroll, S., Vrbora, G., Nicotera, P., Pette, D., Wyss, A., Bluethmann, H., Hunziker, W., and Celio, M. R. (1999) Prolonged contraction-relaxation cycle of fast-twitch muscles in parvalbumin knockout mice, *Am. J. Physiol. 276*, 395−403.
26. Caillard, O., Moreno, H., Schwaller, B., Llano, I., Celio, M. R., and Marty, A. (2000) Role of the calcium-binding protein parvalbumin in short-term synaptic plasticity, *Proc. Natl. Acad. Sci. U.S.A. 97*, 13372−13377.
27. Pack, A. K., and Slepecky, N. B. (1995) Cytoskeletal and calcium-binding proteins in the mammalian organ of Corti: cell type-specific proteins displaying longitudinal and radial gradients, *Hear. Res. 91*, 119−135.
28. Henzl, M. T., Shibasaki, O., Comegys, T. H., Thalmann, I., and Thalmann, R. (1997) Oncomodulin is abundant in the organ of corti, *Hear. Res. 106*, 105−111.
29. Sakaguchi, N., Henzl, M. T., Thalmann, I., Thalmann, R., and Schulte, B. A. (1998) Oncomodulin is expressed exclusively by outer hair cells in the organ of corti, *J. Histochem. Cytochem. 46*, 29−39.
30. Palmisano, W. A., Trevino, C. L., and Henzl, M. T. (1990) Site-specific replacement of amino acid residues within the CD binding loop of rat oncomodulin, *J. Biol. Chem. 265*, 14450−14456.
31. Treviño, C. L., Boschi, J. M., and Henzl, M. T. (1991) Interactions between residues in the oncomodulin CD domain influence Ca^{2+} ion-binding affinity, *J. Biol. Chem. 266*, 11301−11308.
32. Williams, T. C., Corson, D. C., Sykes, B. D., and MacManus, J. P. (1987) Oncomodulin. ^{1}H NMR and optical stopped-flow spectroscopic studies of its solution conformation and metal-binding properties, *J. Biol. Chem. 262*, 6248−6256.
33. Henzl, M. T., Agah, S., and Larson, J. D. (2004) Rat α- and β-parvalbumins: A comparison of their pentacarboxylate and site-interconversion variants, *Biochemistry* (in press).
34. Henzl, M. T., Hapak, R. C., and Likos, J. J. (1998) Interconversion of the ligand arrays in the CD and EF sites of oncomodulin. Influence on Ca^{2+} binding affinity, *Biochemistry 37*, 9101−9111.
35. Henzl, M. T., Wycoff, W. G., Larson, J. D., and Likos, J. J. (2002) ^{15}N nuclear magnetic resonance relaxation studies on rat β-parvalbumin and the penta-carboxylate variants, S55D and G98D, *Protein Sci. 11*, 158−173.
36. Fukada, H., and Takahashi, K. (1998) Enthalpy and heat capacity changes for the proton dissociation of various buffer components in 0.1 M potassium chloride, *Proteins 33*, 159−166.
37. Henzl, M. T., Larson, J. D., and Agah, S. (2000) Influence of monovalent cations on rat α- and β-parvalbumin stabilities, *Biochemistry 39*, 5859−5867.
38. Agah, S., Larson, J. D., and Henzl, M. T. (2003) Impact of proline residues on parvalbumin stability, *Biochemistry 42*, 10886−10895.
39. Permyakov, E. A., Medvedkin, V. N., Kalinichenko, L. P., and Burstein, E. A. (1983) Comparative study of physiochemical properties of two pike parvalbumins by means of their intrinsic tyrosyl and phenylalanyl fluorescence, *Arch. Biochem. Biophys. 227*, 9−20.
40. Thépaut, M., Strub, M.-P., Cavé, A., Banères, J.-L., Berchtold, M. W., Dumas, C., and Padilla, A. (2001) Structure of rat parvalbumin with deleted AB domain: implications for the evolution of EF hand calcium-binding proteins and possible physiological relevance, *Proteins 45*, 117−128.

BI049254D